Journal of Alloys and Compounds 505 (2010) 81–85

Contents lists available at ScienceDirect

Journal of Alloys and Compounds

journal homepage: www.elsevier.com/locate/jallcom

Formation of B19′ martensite in annealed $Ti_{44.6}Ni_{40.1}Cu_{15.3}$ thin films and their shape recovery characteristic

Z.Y. Gao*, M. Sato, A. Ishida

National Institute for Materials Science, Sensor Materials Center, 1-2-1, Sengen, Tsukuba 305-0047, Japan

ARTICLE INFO

Article history:
Received 10 May 2010
Received in revised form 31 May 2010
Accepted 2 June 2010
Available online 11 June 2010

Keywords:
Ti–Ni–Cu
Shape-memory-alloy
Thin film
Microstructure

ABSTRACT

The microstructure and shape memory behavior of $Ti_{44.6}Ni_{40.1}Cu_{15.3}$ thin films annealed at 773, 873, 973 K for 1 h were investigated. The $Ti(Ni,Cu)_2$ particles precipitated in the grain boundaries and grain interiors. As the annealing temperature increased, the grain boundary precipitates became prominent. With increasing annealing temperature, the size of the precipitates increased while the density of precipitates decreased. Unexpected B19′ martensite formed in the annealed thin films, resulting from the composition variation in the matrix induced by precipitation process. Both of the maximum recoverable strain and the critical stress for slip decreased with increasing annealing temperature, which was mainly attributed to the coarsening of the $Ti(Ni,Cu)_2$ precipitates.

1. Introduction

Ti–Ni–Cu shape-memory-alloy thin films formed by sputtering are attractive candidates for powerful microactuator materials because of their recoverable strain and narrow temperature hysteresis, both of which are related to the crystallographically reversible martensitic transformation [1–4]. The phase transformation in Ti–Ni–Cu shape-memory-alloys has been extensively studied by many researchers [5–11]. Whereas the addition of Cu slightly changes the transformation temperature, it changes the transformation path and drastically reduces the temperature hysteresis [12]. The addition of 7.5 at.% Cu changes the transformation path into B2 (cubic) → B19(orthorhombic) → B19′ (monoclinic). With further increasing Cu content, the transformation temperature from B19 to B19′ decreases [13–15]. Ti–Ni–Cu thin films with a Cu content of greater than 10% are known to undergo B2 → B19 martensitic transformation, and the recoverable strain of the B2 → B19 transformation is smaller than that of the B2 → B19′ transformation. Recent combinatorial study demonstrated that a much broader composition range of the Ti–Ni–Cu system provides a reversible phase transformation [16]. The present authors have also been carrying out systematic research on the shape memory behavior and microstructure of Ti–Ni–Cu thin films with Cu contents up to 35 at.% and Ti contents of 48.5–51.5 at.% [17–19]. In the present study we investigated the phase structure and microstructure of $Ti_{44.6}Ni_{40.1}Cu_{15.3}$ thin films, and their shape memory behavior was characterized on the basis of the microstructure.

2. Experimental

$Ti_{44.6}Ni_{40.1}Cu_{15.3}$ thin films were deposited on glass substrates with a carrousel-type magnetron sputtering apparatus [17]. Three targets of pure Ti, Ni and Cu were used to obtain the desired compositions, and the DC powers of these targets were 1000, 270 and 77 W, respectively. The substrate temperature was kept at 473 K and the Ar gas pressure was 0.13 Pa. The substrate holder was rotated at 60 min^{-1} to obtain composition homogeneity during sputtering. The deposition was carried out for 2.5 h and the film thickness was 9 μm. The film composition was determined by inductively coupled plasma atomic emission spectroscopy (ICP-AES).

After sputtering, the deposited films were peeled off the glass substrates and then annealed either at 773, 873 or 973 K for 1 h to produce crystallization. These heat treatments were carried out in a vacuum furnace equipped with infrared lamps. Phase structure was determined by a RINT 2500 X-ray diffractometer with Cu Kα radiation. The microstructure of the annealed films was observed with a transmission electron microscope (JEM-2000FXII) at an accelerating voltage of 200 kV. Thin foils for the transmission electron microscopy observation were prepared by double-jet electropolishing in an electrolyte solution consisting of 95 pct acetic acid and 5 pct perchloric acid by volume. The shape memory behavior of the annealed films was also investigated with a small tensile tester equipped with an automatically controlled heater. The size of the samples used for this test was 0.4 mm × 5 mm (gauge portion) and the thickness was 9 μm. This test involved loading a sample at a high temperature, cooling it down to 143 K and then heating it back to the original temperature with a heating/cooling rate of 10 K min^{-1}. A series of strain-temperature measurements under various constant stresses was carried out with one sample by varying the stress from 20 to 120 MPa in steps of 20 MPa and then from 120 to 600 MPa in steps of 40 MPa.

3. Results and discussion

Fig. 1 shows the TEM images of the annealed $Ti_{44.6}Ni_{40.1}Cu_{15.3}$ thin films. The annealing temperature does not affect the grain size

* Corresponding author. Tel.: +81 298 59 2419; fax: +81 298 59 2401.
E-mail address: gao.zhiyong@nims.go.jp (Z.Y. Gao).

0925-8388/$ – see front matter © 2010 Elsevier B.V. All rights reserved.
doi:10.1016/j.jallcom.2010.06.020

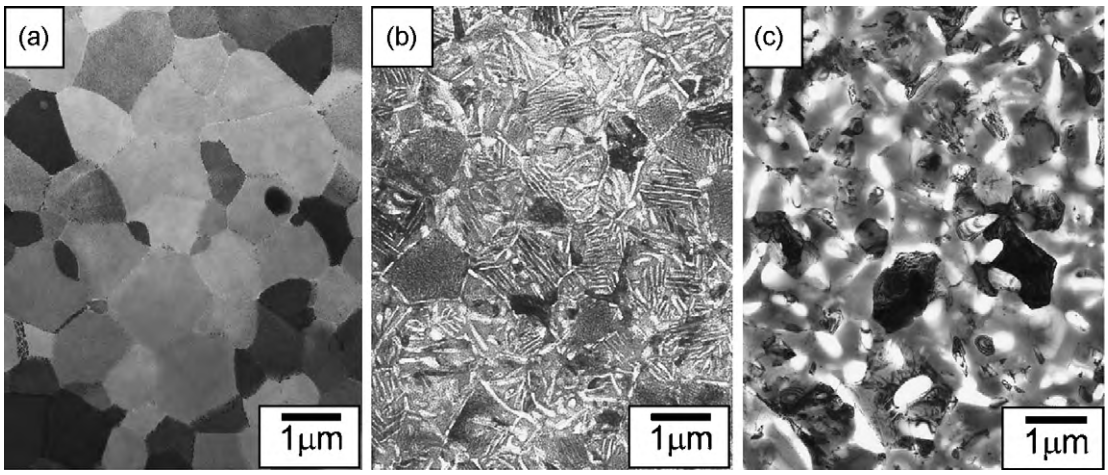

Fig. 1. BF TEM images of the $Ti_{44.6}Ni_{40.1}Cu_{15.3}$ thin films annealed at various temperatures for 1 h (a) 773 K; (b) 873 K; (c) 973 K.

in the films. It can also be found that the precipitates are densely dispersed not only in the grain boundaries but also in the grain interiors for the films annealed at 773 and 873 K for 1 h, whereas there are almost no precipitates within the grains in the films annealed at 973 K. The average size of the precipitates increases with the increasing annealing temperature, and the grain boundary precipitation becomes prominent in the film annealed at 973 K for 1 h.

Fig. 2 shows the microstructures within the grains for the films annealed at 773 and 873 K and their corresponding diffraction patterns in $[1\,0\,0]_{B2}$ orientation; photographs of the film annealed at 973 K were omitted since no precipitates can be observed in the grain interior. One can see plate-like precipitates along the $\langle 1\,0\,0\rangle$ direction of the B_2 matrix, and these precipitates are considered to be a $Ti(Ni,Cu)_2$ phase as will be discussed later. The extra diffraction spots arising from the precipitates cannot be detected in the films annealed at 773 K, probably because the precipitates in the film annealed at 773 K are very small, as verified by the bright field image. The precipitates within the grain lie in the $(0\,1\,0)_{B2}$ and $(0\,0\,1)_{B2}$ planes. These precipitates are very fine and densely distributed in the grain interior in the film annealed at 773 K for 1 h, but the average size of the precipitates increases and the density decreases when the films are annealed at a higher temperature. The average thickness of the precipitates in the film annealed at 773 K for 1 h is estimated to be 1–2 nm, and these precipitates grow almost 10 times in thickness after annealing at 873 K for 1 h. The distance between neighboring precipitates also increases with increasing annealing temperature, suggesting the decrement of the density.

Fig. 3 shows the X-ray diffraction patterns of Ti–Ni–Cu thin films annealed at 773, 873 and 973 K for 1 h. The diffraction patterns were taken at room temperature. Whereas the peaks for the parent phase can be detected in the film annealed at 773 K for 1 h, the diffraction patterns in the $Ti_{44.6}Ni_{40.1}Cu_{15.3}$ thin films annealed at 873 and 973 K for 1 h exhibit a B19′ phase at room temperature. The formation of the B19′ phase is unexpected, since it was reported that Ti–Ni–Cu films with 10 at.% Cu and more undergo a single stage B2 → B19 martensitic transformation. Other than the martensite and parent phase peaks, some additional peaks corresponding to the $Ti(Ni,Cu)_2$ particles can be detected in all the films.

It is known that Ti–Ni–Cu thin films with a Cu content more than 10 at.% undergo a single stage B2 (cubic) → B19 (orthorhombic) martensitic transformation. However, In the present study, the diffraction patterns for B19′ martensite were detected in the films of 15.3 at.% Cu. Meng et al. reported that the B19′ marten-

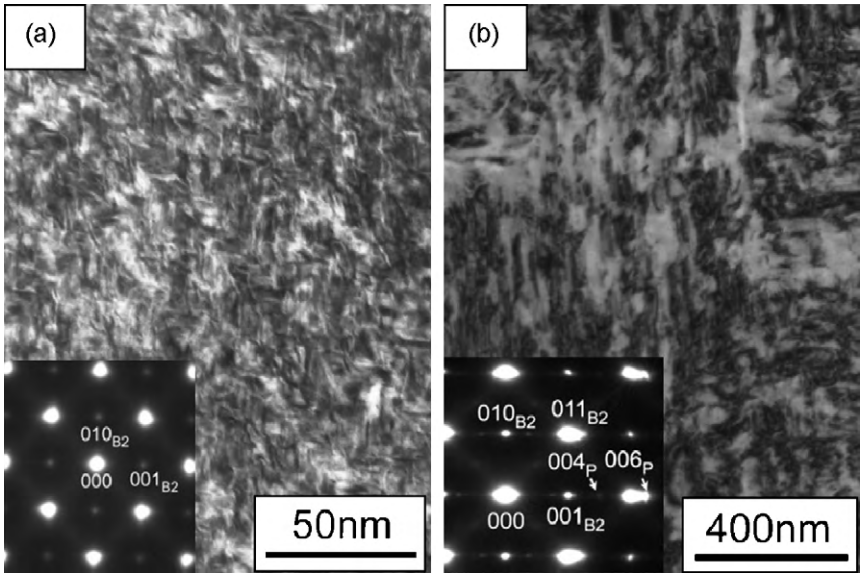

Fig. 2. Bright field images and corresponding diffraction patterns of $Ti_{44.6}Ni_{40.1}Cu_{15.3}$ thin films annealed at (a) 773 K and (b) 873 K. The electron beams were parallel to $[1\,0\,0]_{B2}$.

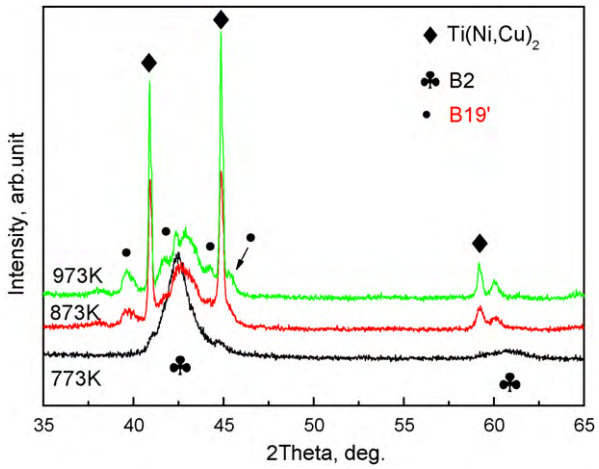

Fig. 3. XRD patterns of annealed $Ti_{44.6}Ni_{40.1}Cu_{15.3}$ thin films at room temperature.

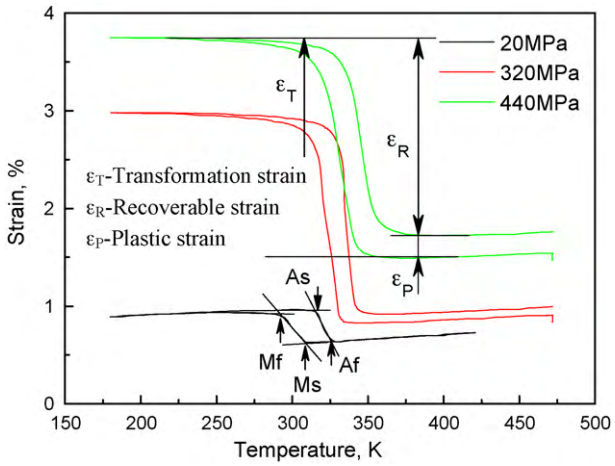

Fig. 5. Strain versus temperature curves measured during heating and cooling under constant stresses for film annealed at 973 K.

site usually appears near the precipitates or grain boundaries in $Ti_{48.6}Ni_{35.9}Cu_{15.5}$ thin films annealed at 873 and 973 K for 1 h as a result of the local strain field near the precipitates and grain boundaries caused by the B2 → B19 transformation, though the reflections from the B19′ phase are not detected in X-ray diffraction patterns [20]. The stress concentration near the precipitates and grain boundaries may explain the formation of the B19′ phase in the films annealed at 973 K where the coarse $Ti(Ni,Cu)_2$ precipitates form. However, we could not find the peaks of B19′ martensite in the XRD results for thin films with higher Cu contents annealed at 973 K for 1 h [21]. It is, therefore, not convincing to attribute the presence of the B19′ martensite to the stress concentration. Zarnetta et al. reported that a $Ti_{39}Ni_{45}Cu_{16}$ thin film decomposed to a TiNi(Cu) phase with a composition of $Ti_{46.0}Ni_{48.5}Cu_{5.5}$ and a $Ti(Ni,Cu)_2$ phase with a composition of $Ti_{33.0}Ni_{44.0}Cu_{23.0}$ after aging at 773–1273 K for 100 h, producing the R-phase transformation [22]. This idea can be applied to the present study. For the present films, the precipitation of $Ti(Ni,Cu)_2$ varies the composition of the matrix towards 50 at.% Ti and low Cu content. This variation in the matrix composition is large when the film composition is far away from the stoichiometric composition. The Cu content of the matrix in the present films is considered to approach less than 7.5 at.% where the B2 → B19′ martensitic transformation takes place.

Fig. 4 shows the annealing temperature dependence of the martensitic transformation start temperature (Ms) under zero stress in the annealing-treated thin films. The Ms under zero stress was evaluated by extrapolating the Clausius–Clapeyron relationship. The Ms increases with the increasing annealing temperature from 773 to 973 K. It is seen that the Ms of the film annealed at 773 K is lower than room temperature, whereas those of films annealed at 873 and 973 K is higher than room temperature. This agrees with the XRD results. The dependence of the martensitic transformation start temperature on the annealing temperature can be explained by the strengthening effect. On the basis of the TEM observation, the size of the $Ti(Ni,Cu)_2$ second phase increases with increasing annealing temperature. As well known, a fine structure strengthens the matrix effectively and, thus, is likely to suppress the shape change associated with the martensitic transformation. This leads to a low transformation temperature.

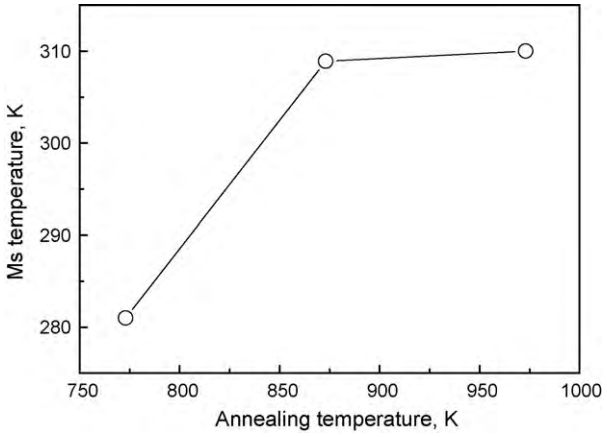

Fig. 4. Annealing temperature dependence of Ms under zero stress in the annealing-treated thin films.

In order to investigate the shape memory behavior in the films, thermal cycling tests between 173 and 423 K under various constant stresses were carried out. Fig. 5 presents the strain vs. temperature curves measured during cooling and heating under a variety of constant stresses in the $Ti_{44.6}Ni_{40.1}Cu_{15.3}$ film annealed at 973 K. It was found that, upon cooling, the specimen starts to elongate at Ms due to the transformation from the parent phase to the martensite phase, and the elongation finishes at the martensitic transformation finish temperature (Mf). Upon heating, the sample starts to shorten at the reverse martensitic transformation start temperature (As) due to the reverse martensitic transformation and the contraction finishes at the reverse martensitic transformation finish temperature (Af). The strain induced here is estimated as the transformation strain (denoted as ε_T). This strain cannot recover completely under high stresses. The residual strain (denoted as ε_P) is attributed to the plastic deformation. The recoverable strain (denoted as ε_R) is defined as the transformation strain minus the plastic strain, as shown in the figure.

Fig. 6 shows the stress dependence of the transformation strain, plastic strain and recoverable strain in a $Ti_{44.6}Ni_{40.1}Cu_{15.3}$ specimen annealed at 873 K for 1 h. The similar behavior is also observed in the other two films. With the increasing stress, the recoverable strain increases due to the volume fraction increasing of the preferentially oriented martensite variants. Under low stresses, a plastic strain is not introduced, indicating a perfect shape recovery. When the stress is higher than the critical stress for slip, a plastic strain is introduced. This critical stress is considered to correspond to the maximum generative stress of an SMA thin-film actuator in that it can recover its original shape up to this stress. The maximum recoverable strain of the film reaches 1.98% at 560 MPa and then decreases owing to the remarkable increase of a plastic strain.

Fig. 7 presents the annealing temperature dependence of the critical stress for slip. The critical stress is determined as the stress

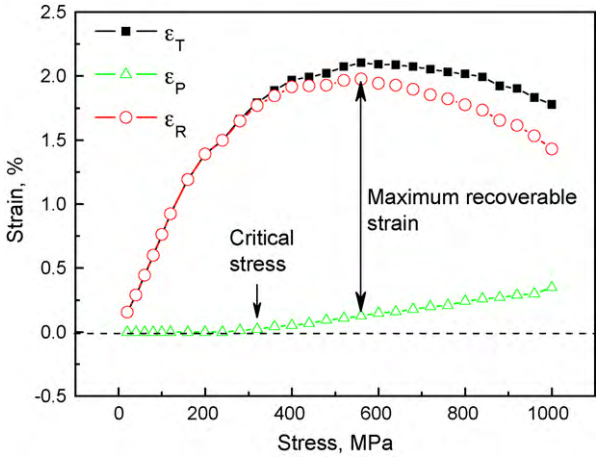

Fig. 6. Shape memory characteristics as a function of stress for $Ti_{44.6}Ni_{40.1}Cu_{15.3}$ annealed at 873 K for 1 h.

below which a plastic strain less than 0.2% is introduced into the specimen. It is seen that the critical stress for slip significantly decreases with the increasing annealing temperature.

From the strain–temperature curves, another important characteristic, i.e. the temperature hysteresis which is determined as the temperature difference between the forward and reverse transformation, was also measured. Fig. 8 shows the temperature hysteresis (Af–Ms) as a function of applied stress for the $Ti_{44.6}Ni_{40.1}Cu_{15.3}$ films annealed at 873 and 973 K. Both the curves can be divided into two regions: the hysteresis of the specimen decreases effectively with the increasing applied stress until the critical stress for slip, and then starts to increase remarkably with the further increasing applied stress. The decrease of the temperature hysteresis is explained by the stress dependence of the forward and reverse transformation temperatures; the former temperature is more sensitive to stress than the latter temperature. And the increase of the temperature hysteresis under high stress may be related to the plastic deformation introduced during thermal cycling. It is considered that the dislocations induced by plastic deformation retard the forward and reverse transformations, thus increasing the temperature hysteresis.

Fig. 9 depicts the annealing temperature dependence of the maximum recoverable strain. Since the thin film annealed at 773 K for 1 h does not show any plastic strain even under the 720 MPa stress (see the inset), it is reasonable to believe that the maximum recoverable strain of the film annealed at 773 K is higher than the

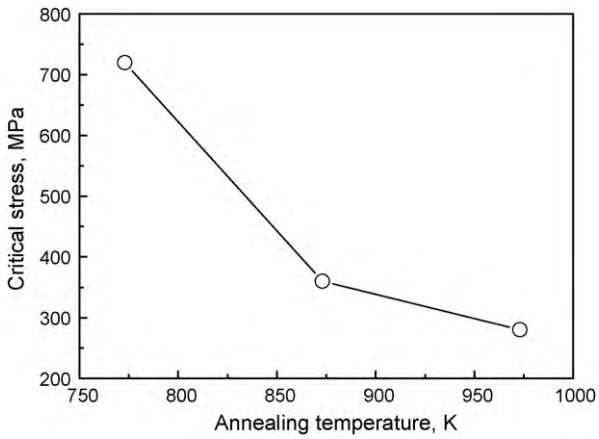

Fig. 7. Effect of annealing temperature on the critical stress for annealed $Ti_{44.6}Ni_{40.1}Cu_{15.3}$ thin films

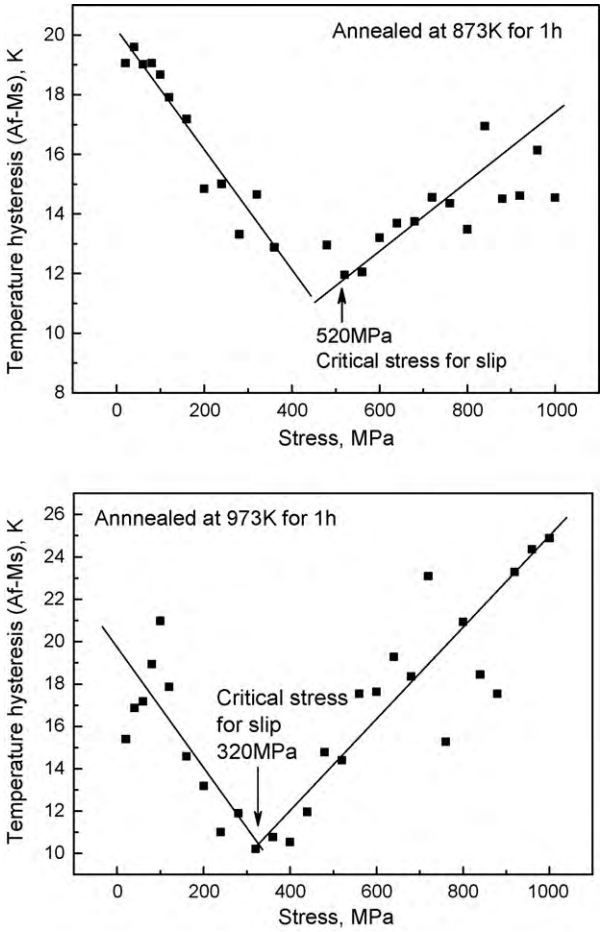

Fig. 8. Effect of stress on the transformation hysteresis of annealed $Ti_{44.6}Ni_{40.1}Cu_{15.3}$ thin films.

recoverable strain of 1.98% obtained under 720 MPa, suggesting that the maximum recoverable strain decreases with the increasing annealing temperature. This decrease of the maximum recoverable strain is caused by both the decrease of a transformation strain and the increase of a plastic strain. It seems that the volume fraction of the B2 phase decreases with increasing annealing temperature. As well known, only the matrix of materials exhibits a shape memory

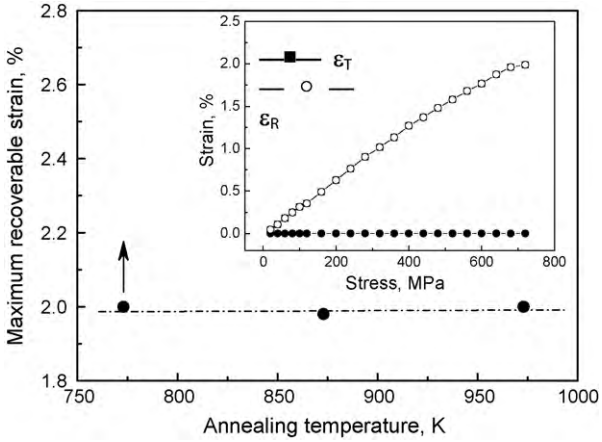

Fig. 9. Annealing temperature dependence of the maximum recoverable strain in the annealed $Ti_{44.6}Ni_{40.1}Cu_{15.3}$ thin films; Inset: stress dependence of the Transformation strain, plastic strain and recovery strain in a specimen annealed at 773 K for 1 h.

effect and contributes to a transformation strain. Moreover, coarse precipitates are likely to restrict the rearrangement of martensite variants and allow for the introduction of dislocations. These cause the decrease of the maximum recoverable strain with the increasing annealing temperature.

4. Conclusions

(1) The $Ti(Ni,Cu)_2$ phase precipitates during the annealing process, and the B19′ martensite is detected in the films annealed at 873 and 973 K for 1 h. The composition variation in the matrix is responsible for the formation of B19′ martensite in the $Ti_{44.6}Ni_{40.1}Cu_{15.3}$ films.
(2) As the annealing temperature increases, the grain boundary precipitates become prominent, and the density of the precipitates within the grains decreases.
(3) With increasing annealing temperature, the martensitic transformation start temperature first increases and then levels off for annealing temperature above 873 K.
(4) Both the maximum recoverable strain and the critical stress for slip significantly decrease with the increasing annealing temperature, which is related to the variation in the microstructure. The $Ti(Ni,Cu)_2$ precipitates play an important role in improving the shape memory effect of $Ti_{44.6}Ni_{40.1}Cu_{15.3}$ films.

References

[1] A. Ishida, V. Martynov, Mater. Res. Soc. Bull. 27 (2002) 111–114.
[2] P. Krulevitch, A.P. Lee, P.B. Ramsy, J.C. Trevino, J. Hamilton, M.A. Northrup, J. Microelectromech. Syst. (1995) 206.
[3] Y.Q. Fu, H. Du, W. Huang, S. Zhang, M. Hu, Sens. Actuators A 112 (2004) 395.
[4] D.D. Shin, K.P. Mohanchandra, G.P. Carman, Sens. Actuators A 119 (2005) 151.
[5] P. Krulevitch, P.B. Ramsey, D.M. Makowiecki, A.P. Lee, M.A. Northrup, G.C. Johnson, Thin Solid Films 274 (1996) 101.
[6] M. Tomozawa, H.Y. Kim, S. Miyazaki, Acta Mater. 57 (2009) 441.
[7] T. Sugawara, K. Hirota, M. Watanabe, T. Mineta, E. Makino, S. Toh, T. Shibata, Sens. Actuators A 130/131 (2006) 461.
[8] Y.Q. Fu, J.K. Luo, A.J. Flewitt, S.E. Ong, S. Zhang, H.J. Du, W.I. Milne, Smart Mater. Struct. 16 (2007) 2651.
[9] B. Winzek, E. Quandt, Z. Metallkd. 90 (1999) 796.
[10] L. Chang, D.S. Grummon, Philos. Mag. A 76 (1997) 163.
[11] Y. Liu, X. Huang, Philos. Mag. 84 (2004) 1919.
[12] M.H. Ren, L. Wang, D. Xu, B.C. Cai, Mater. Des. 21 (2000) 583.
[13] T. Hashinaga, S. Miyazaki, T. Ueki, et al., J. Phys. Paris IV (1995) C8–C689.
[14] S. Miyazaki, T. Hashinaga, A. Ishida, Thin Solid Films 281/282 (1996) 364.
[15] A. Ishida, M. Sato, K. Ogawa, K. Yamada, Mater. Sci. Eng. A 438–440 (2006) 683.
[16] R. Löbel, S. Thienhaus, A. Savan, A. Ludwig, Mater. Sci. Eng. A 481.482 (2008) 151.
[17] A. Ishida, M. Sato, Philos. Mag. 87 (2007) 5523.
[18] A. Ishida, M. Sato, K. Ogawa, Philos. Mag. 88 (2008) 2427.
[19] A. Ishida, M. Sato, Philos. Mag. 88 (2008) 2439.
[20] X.L. Meng, M. Sato, A. Ishida, Acta Mater. 57 (2009) 1525.
[21] Z.Y. Gao, M. Sato, A. Ishida (submitted for publication).
[22] R. Zarnetta, D. Konig, C. Zamponi, A. Aghajani, J. Frenzel, G. Eggelar, A. Ludwig, Acta Mater. 57 (2009) 4169.